J. Phys. B: At. Mol. Opt. Phys. **42** (2009) 095204 (9pp) doi:10.1088/0953-4075/42/9/095204

Electron collision with the silicon monoxide (SiO) molecule using the *R*-matrix method

Hemal N Varambhia[1], Monika Gupta[2], Alexandre Faure[3], K L Baluja[2] and Jonathan Tennyson[1]

[1] Department of Physics and Astronomy, University College London, Gower St., London WC1E 6BT, UK
[2] Department of Physics and Astrophysics, University of Delhi, Delhi 110007, India
[3] Laboratoire d'Astrophysique, UMR 5571 CNRS, Université Joseph-Fourier, BP 53, 38041 Grenoble Cedex 09, France

Received 23 December 2008, in final form 12 February 2009
Published 21 April 2009
Online at stacks.iop.org/JPhysB/42/095204

Abstract
SiO is a molecule that is well known astrophysically. Electron scattering calculations are presented at the static-exchange and close-coupling approximations, one including 24 target states and another including 48 states. Our study predicts the existence of several low-lying narrow $^2\Pi$, $^2\Delta$ and $^2\Sigma^-$ Feshbach resonances and confirms the existence of a $^2\Pi$ bound state. Results from the 48-state close-coupling calculation have been employed to calculate rotational (de)excitation rates and rate-fitting coefficients, which are useful in astrophysical modelling. Ionization cross sections, rotationally summed and resolved differential and integral cross sections are also presented.

(Some figures in this article are in colour only in the electronic version)

1. Introduction

Astrophysicists have had a long-standing interest in SiO and this is reflected by the great number of studies carried out on this molecule confirming its presence in the interstellar medium, e.g. Turner *et al* (1992), Pintado *et al* (1997), Codella *et al* (2002) and Nisini *et al* (2007). Wilson *et al* (1971) first reported on the discovery of silicon monoxide in Sagittarius B2 from line emission spectra and recently Lo *et al* (2007) detected the $J = 2 - 1$ SiO transition from the massive cold dense core G333.125-0.562 and hypothesized that the SiO emission may arise from shocks associated with an outflow in the cold core. Hence the astrophysical motivation for studying SiO has produced a number of *ab initio* quantum chemistry calculations including Cornet and Dubois (1972), Field *et al* (1976), Peterson and Woods (1990), Langhoff and Bauschlicher (1993) and Muniz and Jorge (2006). Peterson and Woods (1990) carried out a configuration interaction study on SiO using diffuse basis sets, with the aim of computing accurate dipole moments and potential energies. Their study employed a CI-SD (all possible single and double electron excitations) level of theory, which yielded a dipole moment of -1.2572 au, in good agreement with the available experimental value of 1.219 au (NIST 2008). Chattopadhyaya *et al* (2003) also performed extensive *ab initio* calculations which are discussed below.

This interest has also resulted in collisional studies being carried out on SiO to calculate rotational excitation rate coefficients, which are widely applied in astrophysical modelling. So far, the majority of research has been focused on atom–SiO collisions: recently Dayou and Balanca (2006) calculated the rotational excitation rates of SiO collisions with the helium atom for all transitions up to $J = 26$ and kinetic temperatures between 10 and 300 K. Their *ab initio* model involved using the coupled-cluster method at the RCCSD(T) level using a very diffuse (aug-pccVQZ) basis set for the Si, O and He atoms to obtain an accurate interaction potential for the He–SiO system. The potential was used to calculate the close-coupled (CC) rotational cross sections and the (de)excitation rates. The data from their He–SiO study were then employed to predict rotational de-excitation rates for impact by para-H_2. Similarly Palov *et al* (2006) calculated rates for rotationally vibrationally inelastic scattering of the hydrogen atom by SiO. Their method involved using an approximate quantum

scattering calculation (vibrational close-coupling rotational infinite order sudden (VCC-IOS) method) of the vibrationally rotationally inelastic scattering cross sections over a relatively large range of scattering energies. Additional work on atom–SiO collision calculations has been carried out by Dickinson and Gottlieb (1970), Bieniek and Green (1981), Bieniek and Green (1983), Sisak and Secrest (1992) and Gusdorf *et al* (2008). However, to date there has been very little work carried out on electron scattering by SiO in the low to medium energy range. This is despite the importance of such interactions in C-type shocks (Jimenez-Serra *et al* 2006) and despite sometimes being the most dominant mechanism of molecular rotational excitation in comets for example (Lovell *et al* 2004); the only electron impact study to have been carried out on SiO was a recent high-energy study by Joshipura *et al* (2007) using a complex potential formalism for the energy range 10–3000 eV. They were unable to benchmark their work in anyway precisely because of the lack of electron impact studies.

The present paper reports on the application of the *ab initio R*-matrix method to low-energy scattering by SiO at the fixed nuclei approximation. In addition to the scattering quantities normally yielded by the *R*-matrix method we have calculated the rotationally resolved differential cross sections and the inelastic rotational integral cross sections as a function of electron energy. These integral cross sections were then employed to calculate the rotational (de)excitation rate coefficients as a function of temperature and their rate-fitting coefficients for later use in astrophysical modelling. To the knowledge of the authors this is the first low-energy electron collision study to have been carried out on SiO.

2. *Ab initio R*-matrix theory

The fixed-nuclei *ab initio R*-matrix theory is based upon the separation of configuration space into two distinct regions—an inner region and an outer region separated by a spherical boundary of radius a, such that it fully contains the electron charge cloud of the molecule and whose centre coincides with the centre of mass of the molecule. In the inner region one solves the $(N+1)$ Hamiltonian eigenvalue problem (N target electrons + 1 scattering electron), where the short-range electron–electron exchange and correlation are the dominant interactions, by employing methods of quantum chemistry. The trial $(N+1)$ scattering eigenfunction is expressed, in common with many other multi-centred scattering methods, as a close-coupling (CC) expansion:

$$\Psi_k^{N+1} = A\sum_i \psi_i^N(x_1, x_2, \ldots, x_N)\sum_j \kappa_j(x_{N+1})a_{ijk} + \sum_l \chi_l(x_1, x_2, \ldots, x_{N+1})b_{lk}, \quad (1)$$

where A is the anti-symmetrization operator, $x_i = \mathbf{r}_i\sigma_i$ is the spin-space co-ordinate of the ith electron, ψ_i^N is the target wavefunction and κ_j is the jth continuum orbital spin coupled with the scattering electron. The expansion coefficients are such that they diagonalize the inner region Hamiltonian to which a Bloch operator needs to be added so as to ensure this Hamiltonian remains Hermitian on the boundary. The first summation yields the target and continuum configurations and the second summation runs over χ_l which are configurations in which all electrons are placed in target occupied and virtual molecular orbitals. These configurations are square integrable or L^2 correlation functions.

The target wavefunctions are usually determined from a CI calculation, where a wavefunction is expanded as a linear combination of configuration state functions (CSFs):

$$\psi_k^N = \sum_i c_{ki}\phi_i^N. \quad (2)$$

The expansion coefficients c_{ki} are such that they diagonalize the target Hamiltonian matrix in the basis of the generated CSFs ϕ_i^N. The target molecular orbitals used to construct the CSFs are optimized using the Hartree–Fock self-consistent field (HF-SCF) method using Gaussian-type orbitals (GTOs). For the polyatomic code the continuum orbitals used here are those of Faure *et al* (2002) and include up to g ($l = 4$) orbitals; unlike those used in the electron-diatomic molecule code (Tennyson and Morgan 1999), these orbitals have no particular boundary conditions. The advantage of using Gaussian-type orbitals is that infinite integrals are then evaluated exactly. The integrals are actually required over the inner region; hence the tail integrals representing the outer region contribution have to be subtracted. This can be done efficiently using property integrals for the short-range GTOs (see Morgan *et al* (1997) for details).

In the outer region, the scattering electron is at a large distance from the centre of mass of the target so the short-range forces so dominant in the inner region are now negligible and the electron is assumed to propagate in the multi-pole potential of the molecule. In the outer region one employs a single centre wavefunction expansion where one can omit the anti-symmetrization operator because the scattering electron occupies a different region of space, and is distinguishable from the target electrons, which always remain in the inner region. Similarly one can also omit the second summation involving the L^2 correlation functions. This yields a set of coupled differential equations which in practice are solved by propagating the *R*-matrix evaluated at the spherical boundary to a large radial distance (Baluja *et al* 1982). These solutions are then matched with the free-wave boundary conditions yielding the *K*-matrix, eigenphase sums, elastic and electronic excitation cross sections.

The UK polyatomic *R*-matrix code only uses Abelian point groups up to and including D_{2h} (Morgan *et al* 1998).

The present paper has made full use of the new JAVA (J2SE) application Quantemol-N (Tennyson *et al* 2007), which provides an interface to the UK Polyatomic *R*-matrix codes (Morgan *et al* 1997). From a few basic user-defined parameters (e.g. molecular cartesian geometry, GTO target basis set, electron energy range and *R*-matrix sphere radius), Quantemol-N can automatically generate a quantum chemistry model and an *R*-matrix scattering model to be used in a particular calculation. In addition to the quantities normally computed by the polyatomic package, the application also computes the BEB (Binary-Encounter-Bethe) ionization cross section (Kim and Rudd 1994, Hwang *et al* 1996). These BEB data are also presented in the paper and compared to the study of Joshipura *et al* (2007).

Table 1. SiO molecular orbital binding and average kinetic energies for DZP basis set and equilibrium geometry. The C_{2v} orbitals are given in the parentheses.

Molecular orbital	$\|B\|$ (eV)	U (eV)	N
1σ ($1a_1$)	1872.68	+2509.7517	2
2σ ($2a_1$)	558.58	+794.7226	2
3σ ($3a_1$)	167.87	+360.8542	2
1π ($1b_1$, $1b_2$)	116.17	+331.3933	4 (2,2)
4σ ($4a_1$)	116.16	+331.8232	2
5σ ($5a_1$)	34.32	+78.1625	2
6σ ($6a_1$)	16.53	+62.1116	2
2π ($2b_1$, $2b_2$)	12.78	+52.1095	4 (2,2)
7σ ($7a_1$)	11.85	+44.1967	2

3. Quantum chemistry model

The present study was carried out using the C_{2v} point group—the highest Abelian sub-group of the natural point group $C_{\infty v}$ and a GTO double zeta-plus-polarization (DZP) basis set for the Si and O atoms. The use of more diffuse basis sets is generally discouraged as the occupied molecular orbitals so obtained would have significant amplitude on the R-matrix sphere surface (typical radius $10\,a_0$). The experimental equilibrium geometry ($r_e = 1.5097$ Å) of the SiO diatomic was employed (NIST 2008). The present study carried out a self-consistent field (SCF) calculation using the above-mentioned basis set and geometry to yield the ground-state electronic configuration $1a_1^2\ 2a_1^2\ 3a_1^2\ 1b_1^2\ 1b_2^2\ 4a_1^2\ 5a_1^2\ 6a_1^2\ 2b_1^2\ 2b_2^2\ 7a_1^2$ ($X\ ^1A_1$) or $1\sigma^2\ 2\sigma^2\ 3\sigma^2\ 1\pi^4\ 4\sigma^2\ 5\sigma^2\ 6\sigma^2\ 2\pi^4\ 7\sigma^2$ ($X\ ^1\Sigma^+$) in the natural point group: the binding energy B, average kinetic energy U and occupation number N of the occupied molecular orbitals obtained by the present study are listed in table 1. By Koopman's theorem the first ionization energy is 11.85 eV which is in good agreement with the experimental value of 11.49 eV (NIST 2008).

The occupied and virtual molecular orbitals obtained using HF-SCF optimization were then used to set up the SiO electronic target states. The study specifically computed complete active space configuration interaction (CASCI) electronic target wavefunctions, as a means of modelling the correlation interaction between the target electrons. The complete active space employed by Quantemol-N was automatically generated: $(1a_1, 2a_1, 3a_1, 1b_1, 1b_2, 4a_1)^{12}$ $(5a_1, 6a_1, 2b_1, 2b_2, 7a_1, 3b_1, 3b_2, 8a_1, 9a_1)^{10}$, namely, 12 electrons (1s, 2s and 2p electrons in the Si atom and the 1s electrons in the O atom) were frozen in all configurations and ten electrons were free to move in the 5–9a_1, 2–3b_1, 2–3b_2 orbitals. This active space yielded 1436 configurations for the $^1A_1$ ($^1\Sigma^+$) ground state. Two target models were analysed: one computed $m = 6$ target Hamiltonian eigenvalues per state and the second involved computing $m = 3$ eigenvalues per state; where m is the number of eigenvalues per electronic state.

We compare our excitation energies with Chattopadhyaya *et al* (2003) who reported an extensive configuration interaction study of the low-lying electronic states of SiO which used *ab initio* based multireference singles and doubles configuration interaction calculations including the core potentials of the Si and O atoms. They also computed the T_e, r_e and ω_e spectroscopic constants of the bound $\Lambda - S$ states of the molecule, and dipole moment μ of the $X\ ^1\Sigma^+$, a $^3\Sigma^+$, b $^3\Pi$, A $^1\Pi$ and E $^1\Sigma^+$ target states. Chattopadhyaya *et al* (2003) used the same complete active space as the present study with ten electrons in the active space. The HF-SCF molecular orbitals set used in their study were computed as a function of bond length using a very diffuse basis set. Table 2 shows the vertical excitation data calculated by the present study compared to the adiabatic and vertical excitation energy data of Chattopadhyaya *et al* (2003) and the experimental work summarized by Herzberg and Huber (1979). It can be seen that our vertical excitation energies are systematically higher than the adiabatic data of the two previous studies, as expected, but are in better agreement with the vertical excitation energy data of the previous theoretical study of Chattopadhyaya *et al* (2003). There are some notable differences between the present and the two previous studies: the low-lying $^1\Delta$ state predicted by Chattopadhyaya *et al* (2003) and reported by Herzberg and Huber (1979) does not appear in our study; conversely, states such as the $2\ ^1\Sigma^-$ predicted by the present study are not predicted by the two previous studies. Considering graph (a) in figure 1 of Chattopadhyaya *et al* (2003) it is interesting to observe that the lowest C $^1\Sigma^-$ and D $^1\Delta$ potential energy curves almost lie on top of each other. At the equilibrium geometry they are indistinguishable. Given this, it might be the case that the

Table 2. SiO vertical excitation energies in eV for all states below the ionization threshold. The target states are designated in $C_{\infty v}$ (C_{2v}) symmetry. The electronic states $4\ ^3\Pi$ onwards do not appear in the $m = 3$ target model. Also shown are the target absolute ground state energy of the present study in E_h and the dipole moment.

Target State	Present work	Experiment[a]	Theory[b] Adiabatic	Theory[b] Vertical
$X\ ^1\Sigma^+$	−363.8534			
$1\ ^3\Pi$ ($^3B_1$, $^3B_2$)	4.64	4.20	4.26	4.29
$1\ ^3\Sigma^+$ ($^3A_1$)	5.11	4.18	4.17	4.74
$1\ ^3\Delta$ ($^3A_1$, $^3A_2$)	5.43	4.53	4.58	5.31
$1\ ^3\Sigma^-$ ($^3A_2$)	5.61	4.76	4.70	5.76
$1\ ^1\Sigma^-$ ($^1A_2$)	5.81	4.80	4.71	5.98
$1\ ^1\Delta$ ($^1A_1$, $^1A_2$)		4.82	4.84	5.98
$2\ ^1\Sigma^+$ ($^1A_1$)	6.13	6.57	6.58	8.02
$1\ ^1\Pi$ ($^1B_1$, $^1B_2$)	6.15	5.32	5.45	5.98
$2\ ^1\Sigma^-$ ($^1A_2$)	7.30			
$2\ ^3\Pi$ ($^3B_1$, $^3B_2$)	8.03		7.11	7.62
$3\ ^1\Sigma^+$ ($^1A_1$)	8.48			
$2\ ^3\Sigma^+$ ($^3A_1$)	8.54	7.15	7.02	7.17
$3\ ^3\Pi$ ($^3B_1$, $^3B_2$)	8.93			
$2\ ^1\Pi$ ($^1B_1$, $^1B_2$)	9.06		7.91	9.15
$3\ ^1\Pi$ ($^1B_1$, $^1B_2$)	10.0			
$2\ ^3\Sigma^-$ ($^3A_2$)	10.1			
$4\ ^3\Pi$ ($^3B_1$, $^3B_2$)	10.3			
$4\ ^1\Sigma^+$ ($^1A_1$)	10.9			
$5\ ^3\Pi$ ($^3B_1$, $^3B_2$)	11.5			
$3\ ^3\Sigma^+$ ($^3A_1$)	11.7	8.45	8.33	
$4\ ^1\Pi$ ($^1B_1$, $^1B_2$)	11.8			
μ/D	2.97	3.1[c]	3.03	

[a] Herzberg and Huber (1979).
[b] Chattopadhyaya *et al* (2003).
[c] NIST (2008).

present study has not included a sufficient number of $^1A_2$ and $^1A_1$ states for the $^1\Delta$ state to appear, or that the $^1\Sigma^-$ may in fact be the $^1\Delta$ but for the absence of the required degenerate $^1A_1$ electronic state. Chattopadhyaya *et al* (2003) and Herzberg and Huber (1979) only considered states below 9.15 eV, so it is not possible to confirm the accuracy of our target states that are above this ceiling, although the general trend observed for states below 9.15 eV suggests that our excitation energies above this will be upper bounds on the true values.

The present study has also calculated states at and above the ionization threshold (not shown in table 2). Such states are useful for representing polarization effects; they are better represented using pseudo-continuum orbitals (Gorfinkiel and Tennyson 2004, Tarana and Tennyson 2008), which was not attempted here. These high-lying states do not have any physical significance but were nevertheless included in our scattering model as discussed below.

The ground-state dipole moment of the present work is in very good agreement with the experimental value (NIST 2008) and the theoretical value of Chattopadhyaya *et al* (2003) (3.03 D) but it is much higher than the MP4 study of Maroulis *et al* (2000). A Hartree–Fock SiO wavefunction was also computed, resulting in a much higher dipole moment of 3.7 D.

The polarizability tensor gives a good indication of how well the polarization interaction will be modelled in the outer region. In the present work, the diagonal components α_{xx}, α_{yy} and α_{zz} were computed using first-order perturbation theory. From this the mean spherical polarizability, α_0, was found to be 18.5 a_0^3 for the $m = 6$ target model. The highest value of the polarizability of Maroulis *et al* (2000) was 28.02 a_0^3. There does not appear to be any experimental value of the mean polarizability to which we might able to compare.

4. Scattering model

All scattering models employed the GTO continuum basis set of Faure *et al* (2002) to model the scattering electron and a partial wave expansion up to and including g-partial wave ($l \leqslant 4$). These continuum orbitals were orthogonalized to the target molecular orbitals using a mixture of Schmidt and Loewden symmetric orthogonalization methods, and those continuum orbitals with an overlap of less than 2×10^{-7} were removed. Since SiO is a very polar diatomic, the convergence of the continuum orbital partial wave expansion is very slow therefore in the present study the higher partial waves that are excluded from the continuum orbitals were accounted for using the Born correction (Kaur *et al* 2008).

By virtue of the two target models investigated, two scattering models were also studied which varied the number of target states included in the close-coupling expansion and retained for the construction of the *R*-matrix at the surface of the sphere. A static-exchange (SE) calculation was also carried out to determine the nature of any resonances, whether they were shape resonances or Feshbach ones. For all the studies carried out, some of the low-lying virtual molecular orbitals calculated from the SCF calculation were used to augment the continuum basis set. These orbitals allow for high partial waves in the region of the nuclear singularity; however as they do not extend in the outer region they do not assist with the slow convergence of the partial wave expansion due to the effects of the long-range dipole potential.

Initial calculations used a sphere radius of 10 a_0. However, it was found that there was significant amplitude on the spherical boundary (arising from the occupied molecular orbitals) so this radius was increased to 12 a_0, which reduced the most significant orbital amplitude from order 10^{-4} to order 10^{-6}.

In order to preserve the balance between the amount of correlation incorporated in the target wavefunction and in the scattering calculation, 11 electrons (ten target electrons and one scattering electron) were allowed to move freely amongst the $5a_1$, $6a_1$, $2b_1$, $2b_2$, $7a_1$, $3b_1$, $3b_2$, $8a_1$ and $9a_1$ target occupied and virtual orbitals.

Test calculations were carried out which included 24 states (150 channels) in the close-coupling expansion and retention of the same in the outer region for the construction of the *R*-matrix on the sphere boundary. In addition, calculations were carried out using 48 target states (300 channels). The reason for including so many states was so as to improve the modelling of the polarization interaction, which, *ab initio*, is modelled by the retention of a large number of closed electronic excitation channels. So far as computational efficiency is concerned, the computation time for the outer region becomes longer due to the increased size of the large open-closed portion of the *R*-matrix. The computer time for the calculation of the $(N+1)$-trial scattering wavefunction however, remains unaffected by the inclusion of more target states (Tennyson 1996).

Finally all calculations were carried out on the $^2A_1$, $^2A_2$, $^2B_1$ and $^2B_2$ scattering symmetries and for the incident electron energy range 0.02 eV–10.0 eV. For matching to the asymptotic form of the reduced radial wavefunction of the scattered electron, and hence the computation of the *K*-matrix, the *R*-matrix was propagated to a radial distance of 100.1 a_0.

5. Results

The present study computed the multichannel eigenphase sum, the inelastic cross section, total cross section, rotationally resolved differential cross sections (DCSs) for incident energies 1 eV, 2 eV, 3 eV and 4 eV, rotationally inelastic integral cross sections and rotational rates for all transitions up to $J = 40$. Here the best model was taken to be the 48-state CC model, and the results for these are discussed below. Quantemol-N also computed the Binary-Encounter-Bethe (BEB) ionization cross section using the molecular orbitals listed in table 1 and a dipole constant, Q, set to unity for each orbital. A number of interesting phenomena were observed in the low-energy scattering data which are discussed below. The scattering model employed in the present study has no influence upon the BEB ionization cross section calculated by Quantemol-N except the GTO basis set employed to construct the occupied and virtual molecular orbitals.

5.1. Eigenphase sums, resonances and bound states

For both the static exchange calculation and the *N*-state close-coupling (CC) calculations, the $^2A_1$ eigenphase sums of the

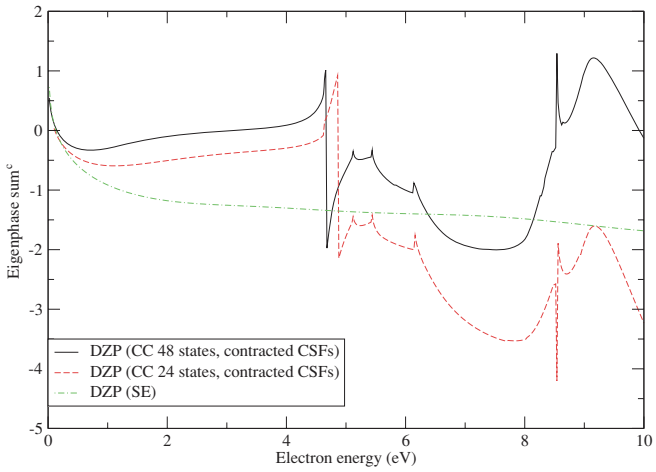

Figure 1. Comparison of the SiO $^2A_1$ (predominantly $^2\Sigma^+$) eigenphase sums.

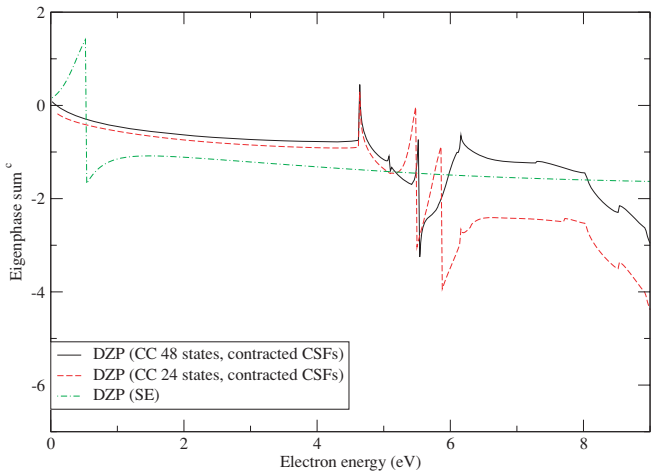

Figure 2. Comparison of the SiO $^2B_1$ (predominantly $^2\Pi$) eigenphase sums.

present study in figure 1 show a very sharp upturn as the electron energy tends to zero. This is a characteristic typical of dipole bound states and is predicted by Levison's theorem. Some of the stuctures shown in the close-coupling eigenphase sum curves are absent from the static exchange and this is because these features represent the opening up of new excitation channels (table 2). Resonances manifest themselves in plots of eigenphase sums as a rapid increase of π in the eigenphase; given that the eigenphase is arbitrary modulo π, resonances, particularly when narrow, often actually appear as seeming discontinuities in these plots. Figure 1 also appears to show a narrow resonance feature at approximately 4.5–4.7 eV which is also absent from the static exchange eigenphase, indicating that this may be a Feshbach. The $^2A_2$ eigenphase sum curve (not shown) also shows a similar resonance feature at the same position, meaning that this Feshbach resonance has $^2\Delta$ symmetry. It is also to be noted that as more states are included in the CC expansion and retained in the outer-region calculation, the eigenphase sum increases—this is a clear indication of the improved modelling of the polarization interaction.

The $^2B_1$ eigenphase sums presented in figure 2 are also notable in terms of structure: the SE calculation shows a resonance feature below 1 eV which disappears when one employs the CC expansion. This behaviour is typical of a weakly bound state. In addition the R-matrix poles E_{N+1} were calculated for each scattering symmetry and the $^2\Pi$ R-matrix pole was found to be $-363.8601E_h$, slightly lower than the target ground state ($-363.8534E_h$) and so also corresponds to a bound state of $^2\Pi$ symmetry. This and the disappearance of the $^2\Pi$ SE shape resonance very neatly confirm the density functional study of Alikhani *et al* (1997). The 48-state CC model predicts that this bound state lies at position -0.12 eV compared to -0.16 eV by Alikhani *et al* (1997). Our study also predicts the existence of very narrow $^2\Pi$ Feshbach resonances between 5 and 6 eV. The position E_r and width Γ_r parameters of the Feshbach resonances yielded by the close-coupled calculations are given in table 3. These parameters were obtained by fitting to the Breit–Wigner profile (Tennyson and Noble 1984). The parameters of a Feshbach resonance are very sensitive to the treatment of the polarization interaction. Table 3 confirms the effect of the improved modelling of the polarization interaction, namely the lowering of the position and the narrowing of the width: in the case of the $^2\Delta$ Feshbach resonance, the width is more than halved by the retention of 24 additional states and the position is lowered by about 3%. It is interesting to note that the 48-state CC model predicts the existence of three $^2\Pi$ and one $^2\Sigma^-$ Feshbach resonances (the latter arising from the $^2A_2$ eigenphase curve) whereas the 24-state model predicts only one $^2\Pi$ and does not predict a $^2\Sigma^-$ resonance at all. This may be another effect of improved modelling, but since we have conducted no further studies retaining more than 48 states this is difficult to confirm.

Table 3. Resonances for the 48-state and 24-state SiO close-coupling model. The parameters are given in eV.

	$N = 48$		$N = 24$	
Symmetry	E_r	Γ_r	E_r	Γ_r
$^2\Pi$	5.09	0.0029		
$^2\Pi$	5.53	0.0586		
$^2\Pi$	5.96	0.343	5.72	0.357
$^2\Delta$	4.69	0.250	4.82	0.593
$^2\Sigma^-$	8.16	0.411		

5.2. *Inelastic and ionisation cross sections*

The electronic excitation cross sections show some interesting peak structure. Figure 3 shows the inelastic cross sections for electronic excitation to the first four low-lying states $^3\Pi$, $^3\Sigma^+$, $^3\Delta$ and $^3\Sigma^-$ (table 2) for the 48-state CC calculation. The X $^1\Sigma^+ \rightarrow {}^3\Pi$ excitation cross section shows a pronounced double peak structure below 5 eV. Analysis of the partial cross sections suggests that lower peak is caused by the $^2\Delta$ Feshbach resonance shown in table 3 whereas the second peak is simply caused by the rapid rise in the $^2\Sigma^+$ cross section often found near threshold for spin changing excitations. There is also a sharp narrow peak at around 5.5 eV in the X $^1\Sigma^+ \rightarrow {}^3\Delta$

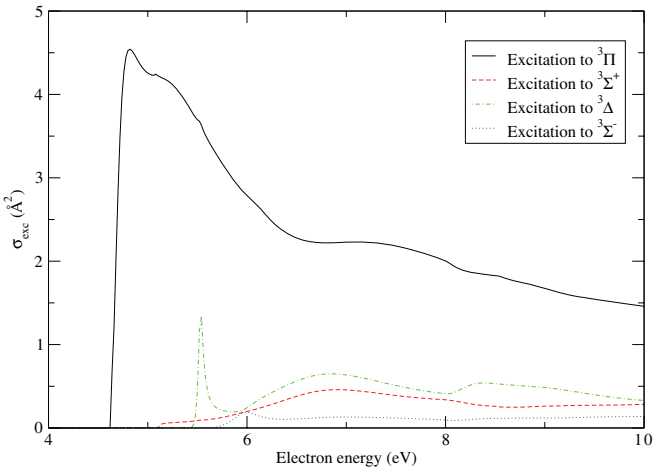

Figure 3. SiO electronic excitation cross sections to the first four lowest lying electronic excitation channels for the 48-state close-coupling model.

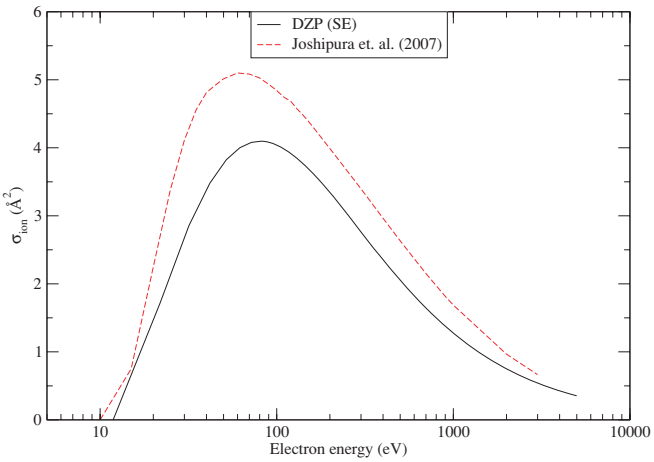

Figure 4. Comparison of the Quantemol-N SiO BEB ionization cross section to the calculation of Joshipura *et al* (2007).

excitation cross section which might correspond to the second of the three $^2\Pi$ Feshbach resonances in table 3. A smaller and wider peak appears at about 6 eV in the X $^1\Sigma^+ \rightarrow {}^3\Sigma^-$ cross section which could well correspond to the third of the three $^2\Pi$ resonances. Finally it is interesting to note the presence of a broad peak in the X $^1\Sigma^+ \rightarrow {}^3\Delta$ cross section at about 8.2 eV which coincides with the position of the $^2\Sigma^-$ resonance.

Figure 4 shows the electron impact ionization cross section of SiO computed by the present study alongside the complex potential formalism calculations of Joshipura *et al* (2007). Quantemol-N computed the ionisation cross section for the ith C_{2v} molecular orbital (table 1) using the standard formula (Kim and Rudd 1994) and then by summing over these occupied orbitals. It can be seen from figure 4 that the data of Joshipura *et al* (2007) are systematically higher than our BEB data over the entire energy range considered. Given the absence of other high-energy electron collision theoretical or experimental data, it is difficult to draw any sort of conclusion. It is true to say that the BEB formalism has consistently yielded cross sections that are in very good agreement with experiment (see http://physics.nist.gov/PhysRefData/Ionization/molTable.html for example). The BEB cross section is sensitive to the precise value of the ionization energy employed and in nearly all calculations the experimental value has been adopted so as to attain agreement with experiment. This strategy was tested in the present study and since the ionization energy of the present study (11.85 eV) is in good agreement with experiment (11.49 eV, NIST (2008)), little difference in the ionization cross section was found.

5.3. Rotational differential cross section and integral cross sections

For all the figures shown in this section the 48-state CC T-matrices were employed in their calculation.

Initially the T-matrices were transformed from their C_{2v} representation to that of the natural point group $C_{\infty v}$ to yield a new set of linear T-matrices for the $^2\Sigma^+, {}^2\Pi, {}^2\Delta, {}^2\Phi$ and $^2\Gamma$ scattering symmetries, using the mappings $m_{l_i} = 0 \rightarrow \Sigma^+, m_{l_i} = 1 \rightarrow \Pi, m_{l_i} = 2 \rightarrow \Delta, m_{l_i} = 3 \rightarrow \Phi$ and $m_{l_i} = 4 \rightarrow \Gamma$ for a $^1\Sigma^+$ ground-state molecule. Here m_{l_i} is the z-projection of the scattering electron partial wave l_i for the ith channel. This new set was then employed in the calculation discussed below.

In this approach the cross section is written as a sum over partial waves within the adiabatic nuclei rotation (ANR) approximation, which assumes that the rotational excitation channels are degenerate. For low partial waves (here defined as $l \leqslant 4$) T-matrices computed from the R-matrix calculations are employed to compute the cross section. In the case of dipole-forbidden excitations ($\Delta J \neq 1$) the convergence of the cross-sectional partial wave expansion is expected to be rapid hence it may be evaluated using the FN T-matrices alone; in the case of the dipole-allowed excitations ($\Delta J = 1$) the partial wave expansion converges slowly owing to the long-range nature of the dipole interaction. In order to account for the higher partial waves not included in the FN T-matrices, the Born correction was applied. Hence the low partial wave contribution is included via the R-matrix calculation and the Born correction. The low partial waves contribution arising from the Born contribution is therefore subtracted in order that the final rotational cross section set only contains those low partial waves due to the R-matrix calculation. It was found from the previous study of Faure *et al* (2007) that quadrupole and induced dipole Born completion was negligible so it was not included in the present study either. The restriction of the ANR approximation is that it is only reliable at collision energies where the collision time becomes appreciable compared to the time period of nuclear rotational motion (Feldt and Morrison 1982). SiO has its first inelastic threshold at 4.63 eV so the computation of the inelastic rotational cross section was restricted to the range 0.02–4.6 eV. Excitation cross sections were extrapolated at very low energy, down to threshold as in Faure *et al* (2007).

For strongly dipolar systems, the differential cross sections (DCSs) are more accurately measured than integral cross sections (Faure *et al* 2004). As a test of the accuracy

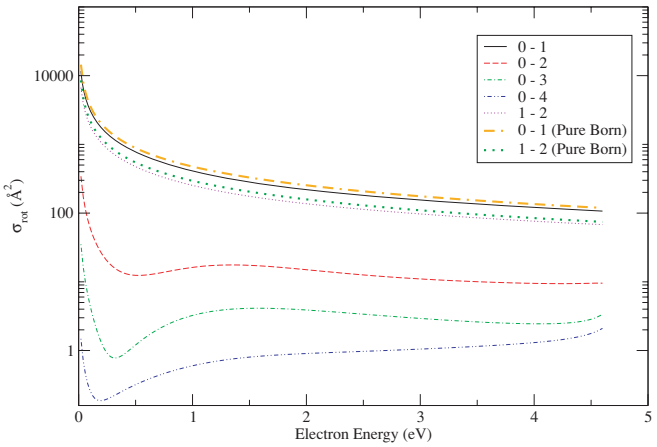

Figure 5. SiO rotationally inelastic cross sections for incident electron energies below 4.6 eV.

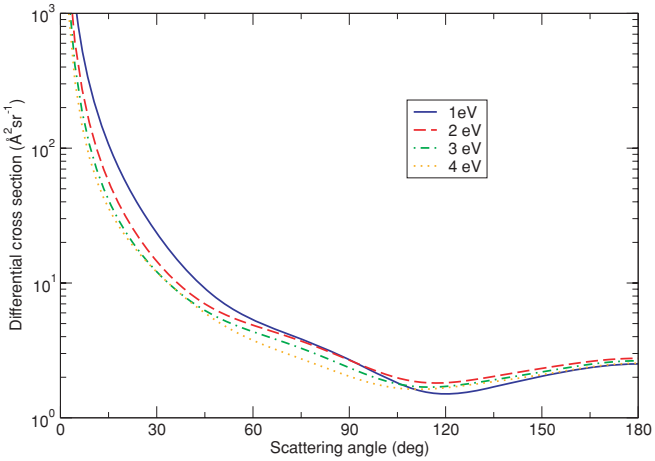

Figure 6. SiO rotationally summed differential cross sections for incident energies 1 eV, 2 eV, 3 eV and 4 eV.

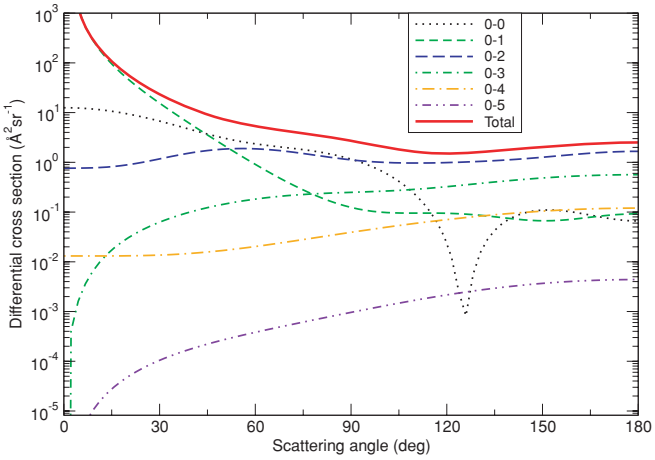

Figure 7. SiO rotationally resolved and summed differential cross sections for incident energy 1 eV.

of a theoretical model one would usually compare calculated differential cross sections to those of experiment. The present study cannot carry out this bench mark test as no such experimental data exist. However they can be made available on application to the authors. To confirm the validity of our treatment, we compared the ANR integral rotational cross sections obtained using the FN T-matrices to the cross sections obtained by the angular integration of the DCSs obtained using the Born closure approach (Itikawa 2000) and both coincided to within 1%.

Figure 5 shows the rotational integral cross sections as a function of energy and it may be noticed that the dipole allowed cross sections 0–1 and 1–2 dominate over the dipole fobidden 0–2 by almost two orders of magnitude, a reflection of the large dipole moment of SiO. Similar results were observed for HCN (Faure *et al* 2007). As shown in figure 5, these $\Delta J = 1$ cross sections are close to but slightly overestimated by the pure dipole Born calculations.

Figure 6 shows the rotationally summed DCSs for incident energies 1 eV, 2 eV, 3 eV and 4 eV. It is interesting to observe the appearance of two shoulder features at about 60° and 120° which would seem to indicate that for these energies scattering is chiefly s-, p- and d-wave in nature. The 1 eV DCS in particular is studied in more detail in figure 7 which shows the summed and the J-resolved differential cross sections for this energy, and a general trend can be inferred. The divergence at the forward angle is confirmed as being due to the dipole-allowed transition 0–1 dominating the scattering. This begins to decline in importance beyond about 50°. The slight shoulder feature at around 60° appears to be due to the temporarily dominant 0–0 elastic DCS and the maximum in the 0–2 DCSs between 60° and 70° dominating over the 0–1 DCS. The shoulder feature at 120° seems to arise due to the slight upturn in the 0–2 differential cross section and the increased contribution of the 0–3 transition. At the backward angles the dipole forbidden 0–2 and 0–3 transitions are now dominant, especially 0–2. The elastic 0–0 differential cross section also exhibits a pronounced dip at around 130° which may be attributed to rainbow scattering.

6. Rotational rates

Rotational rate coefficients were obtained for the temperature range 5–5000 K for all transitions up to and including $J = 40$ using a Maxwellian velocity distribution for the electron. For use in astrophysical modelling, the temperature dependence of the downward transition rates $k(T)$ (units cm^3 s^{-1}) were fitted to the analytic form:

$$\log_{10} k(T) = \sum_{r=0}^{N} a_r x^r, \tag{3}$$

where $x = T^{-1/6}$ and $N = 4$.

The fitting coefficients are listed in table 4 and the graph of the excitation rates for the dipole-allowed transitions $J = 0$–1 and $J = 1$–2 and the dipole forbidden $J = 0$–2 is given in figure 8. Coefficients for $J > 8$ can be obtained upon request from the authors.

Although there has been no other study carried out on electron impact rotational excitation of SiO, we have chosen to compare our excitation rates with the atom–SiO data of Dayou and Balanca (2006) and Palov *et al* (2006). The

Table 4. SiO rotational rate-fitting coefficients obtained for the 48-coupled states calculation. Coefficients for $J > 8$ can be obtained upon request from the authors. The energies E_{up} are from the CDMS catalogue as given in http://www.strw.leidenuniv.nl/~moldata/datafiles/sio.dat.

Transition	$E_{up}(K)$	a_0	a_1	a_2	a_3	a_4
(1 − 0)	2.1	−7.731	11.928	−22.532	18.395	−5.200
(2 − 0)	6.3	−10.395	14.975	−23.728	16.558	−3.819
(2 − 1)	6.3	−7.656	11.869	−23.242	20.127	−6.326
(3 − 0)	12.5	−11.600	11.999	−6.300	−14.916	14.215
(3 − 1)	12.5	−10.178	14.027	−20.606	11.987	−1.533
(3 − 2)	12.5	−7.603	11.605	−22.991	20.254	−6.547
(4 − 0)	20.8	−0.013	−91.311	293.200	−391.836	187.661
(4 − 1)	20.8	−11.386	11.195	−3.625	−18.944	16.301
(4 − 2)	20.8	−10.127	13.935	−20.098	10.828	−0.807
(4 − 3)	20.8	−7.596	11.643	−23.568	21.388	−7.218
(5 − 0)	31.3	0.278	−101.271	306.022	−391.605	181.361
(5 − 1)	31.3	0.227	−92.165	295.804	−395.563	189.546
(5 − 2)	31.3	−11.255	10.466	−1.111	−22.809	18.348
(5 − 3)	31.3	−10.067	13.584	−18.811	8.690	0.371
(5 − 4)	31.3	−7.581	11.584	−23.815	22.083	−7.682
(6 − 0)	43.8	−1.067	−101.243	292.697	−362.114	163.215
(6 − 1)	43.8	0.412	−101.110	305.389	−391.001	181.190
(6 − 2)	43.8	0.421	−93.236	298.996	−399.926	191.696
(6 − 3)	43.8	−11.182	10.104	0.015	−24.476	19.196
(6 − 4)	43.8	−10.036	13.439	−18.270	7.709	0.932
(6 − 5)	43.8	−7.583	11.646	−24.360	23.082	−8.256
(7 − 0)	58.3	11.481	−239.733	742.962	−980.050	467.243
(7 − 1)	58.3	−0.977	−100.479	289.822	−358.180	161.327
(7 − 2)	58.3	0.444	−100.663	303.710	−388.754	180.127
(7 − 3)	58.3	0.555	−93.980	301.082	−402.672	193.010
(7 − 4)	58.3	−11.069	9.271	2.732	−28.409	21.210
(7 − 5)	58.3	−10.010	13.327	−17.931	7.135	1.242
(7 − 6)	58.3	−7.561	11.498	−24.229	23.190	−8.410
(8 − 0)	75.0	−11.286	−8.395	−54.348	142.094	−90.529
(8 − 1)	75.0	11.916	−242.005	749.537	−988.557	471.274
(8 − 2)	75.0	−1.069	−98.999	285.134	−352.177	158.564
(8 − 3)	75.0	0.464	−100.350	302.442	−387.001	179.279
(8 − 4)	75.0	0.665	−94.637	302.945	−405.165	194.232
(8 − 5)	75.0	−10.985	8.646	4.744	−31.332	22.724
(8 − 6)	75.0	−10.000	13.293	−17.720	6.551	1.661
(8 − 7)	75.0	−7.579	11.687	−25.112	24.596	−9.162

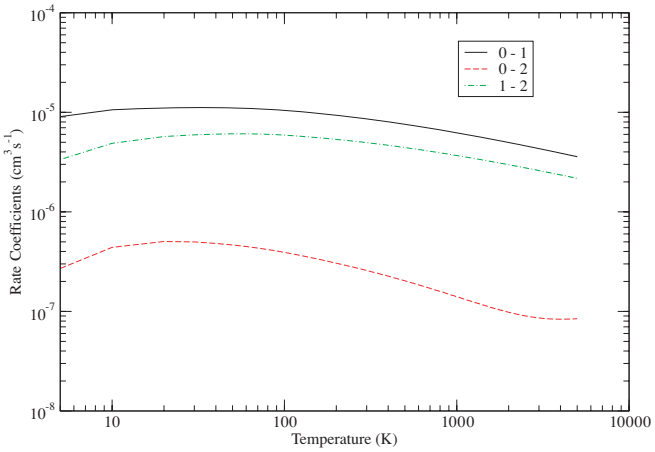

Figure 8. SiO rotational rate coefficients obtained for the 48-state calculation.

rates obtained for collisions with electrons are typically six orders of magitude higher than the He–SiO rate coefficients of Dayou and Balanca (2006), and four to six orders of magnitude higher than the H–SiO rate coefficients of Palov *et al* (2006). One can conclude from this observation that electron collisions can compete with, if not dominate over, atom collisions as the chief rotational excitation mechanism of SiO in astrophysical regions where the ionization degree exceeds $\sim 10^{-5}$ (e.g., diffuse interstellar clouds, C-type shocks, etc). Similar conclusions were reached by Faure *et al* (2007) for HCN.

7. Conclusion

The present study has applied the *ab initio R*-matrix method to low-energy electron impact excitation of SiO, with the aim of calculating quantities of astrophysical interest. This is the first low-energy electron impact study to have been carried out on SiO. Our study employed the configuration interaction and Hartree–Fock methods to represent the target for use in close-coupling and static exchange scattering calculations, respectively. Two *N*-state close-coupling calculations were carried out. The first one retained 24 target states (150 channels) and the second retained 48 target states, or 300 channels in the said expansion and for the construction of the

R-matrix evaluated at the surface of the sphere, the radius of which was taken to be 12 a_0 so as to fully contain the target molecular electron charge cloud.

The scattering quantities computed were the eigenphase sum, the electronic excitation cross section and the Binary-Encounter-Bethe ionization cross section using the HF-SCF occupied molecular orbitals. The *T*-matrices obtained from the *R*-matrix calculation were initially transformed to the natural symmetry $C_{\infty v}$ to yield a new set of *T*-matrices for the scattering symmetries $^2\Sigma^+$, $^2\Pi$, $^2\Delta$, $^2\Phi$ and $^2\Gamma$. These were then employed in the computation of the inelastic rotational cross sections, the rotationally resolved differential cross sections and rate coefficients and their fitting coefficients for all transitions up to $J = 40$, some or all of which may be useful in later astrophysical modelling.

Our study was able to detect some interesting features of the scattering calculation, particularly the independent confirmation of a $^2\Pi$ SiO^- bound state at −0.12 eV which was predicted by the density functional work of Alikhani *et al* (1997). We also predict the existence of low-lying narrow $^2\Pi$ and $^2\Delta$ Feshbach resonances at 5–6 eV and a $^2\Sigma^-$ Feshbach resonance at 8.16 eV. Due to the lack of other low-energy e-SiO scattering studies this work cannot be benchmarked at present. However, it may aid in the detailed investigation of electron density enhancements expected during the first stages of a C-type shock evolution (Jimenez-Serra *et al* 2006), or indeed other astrophysical environments.

Acknowledgments

The authors are grateful to Professor K N Joshipura for providing his ionization cross section data and to Thierry Stoeklin for use of his DCS code. This work was supported by a Royal Society Joint Project Grant.

References

Alikhani M E, Tremblay B and Manceron L 1997 *J. Mol. Struct. (Theochem.)* **394** 25–31
Baluja K L, Burke P G and Morgan L A 1982 *Comput. Phys. Commun.* **27** 299–307
Bieniek R J and Green S 1981 *Chem. Phys. Lett.* **84** 380–4
Bieniek R J and Green S 1983 *Astrophys. J.* **265** 29
Chattopadhyaya S, Chattopadhyay A and Das K K 2003 *J. Phys. Chem.* A **107** 148–58
Codella C, Scappini F, Bachiller R and Benedettini M 2002 *Mon. Not. R. Astron. Soc.* **331** 893–900
Cornet R and Dubois I 1972 *Can. J. Phys.* **50** 630
Dayou F and Balanca C 2006 *Astron. Astrophys.* **459** 297–305
Dickinson D F and Gottlieb C A 1970 *Astrophys. Lett.* **7** 205
Faure A, Gorfinkiel J D, Morgan L A and Tennyson J 2002 *Comput. Phys. Commun.* **144** 224–41
Faure A, Gorfinkiel J D and Tennyson J 2004 *J. Phys. B: At. Mol. Opt. Phys.* **37** 801–7
Faure A, Varambhia H N, Stoecklin T and Tennyson J 2007 *Mon. Not. R. Astron. Soc.* **382** 840–8
Feldt A N and Morrison M A 1982 *J. Phys. B: At. Mol. Opt. Phys.* **15** 301–8
Field R W, Lagerqvist A and Renhorn I 1976 *Phys. Scr.* **14** 298–319
Gorfinkiel J D and Tennyson J 2004 *J. Phys. B: At. Mol. Opt. Phys.* **37** L343–50
Gusdorf A, Cabrit S, Flower D R and des Forets G P 2008 *Astron. Astrophys.* **482** 809–29
Herzberg G and Huber K P 1979 *Molecular Spectra and Molecular Structure* vol 4 (New York: Van Nostrand Reinhold)
Hwang W, Kim Y K and Rudd M E 1996 *J. Chem. Phys.* **104** 2956
Itikawa Y 2000 *Theor. Chem. Acc.* **105** 123–31
Jimenez-Serra I, Martin-Pintado J, Viti S, Martin S, Rodriguez-Franco A, Faure A and Tennyson J 2006 *Astrophys. J.* **650** 135–8
Joshipura K N, Vaishnav B G and Gangopadhyay S 2007 *Int. J. Mass Spectrom.* **261** 146–51
Kaur S, Baluja K L and Tennyson J 2008 *Phys. Rev.* A **77** 032718
Kim Y K and Rudd M E 1994 *Phys. Rev.* A **50** 3954–67
Langhoff S R and Bauschlicher C W 1993 *Chem. Phys. Lett.* **211** 305–11
Lo N, Cunningham M, Bains I, Burton M G and Garay G 2007 *Mon. Not. R. Astron. Soc.* **381** L30–4
Lovell A J, Kallivayalil N, Schloerb F P, Combi M R, Hansen K C and Gombosi T I 2004 *Astrophys. J.* **613** 615–21
Maroulis G, Makris C, Xenides D and Karamanis P 2000 *Mol. Phys.* **98** 481–91
Morgan L A, Gillan C J, Tennyson J and Chen X 1997 *J. Phys. B: At. Mol. Opt. Phys.* **30** 4087–96
Morgan L A, Tennyson J and Gillan C J 1998 *Comput. Phys. Commun.* **114** 120–8
Muniz E and Jorge F 2006 *Int. J. Quant. Chem.* **106** 943–52
Nisini B, Codella C, Giannini T, Garcia J S, Richer J S, Bachiller R and Tafalla M 2007 *Astron. Astrophys.* **462** 163–72
NIST 2008 Computational chemistry comparison and benchmark database, http://cccbdb.nist.gov/
Palov A P, Gray M D, Field D and Balint-Kurti G G 2006 *Astrophys. J.* **639** 204–9
Peterson K A and Woods R C 1990 *J. Chem. Phys.* **92** 6061
Pintado J M, de Vicente P, Fuente A and Planesas P 1997 *Astrophys. J. Lett.* **482** 45
Sisak M and Secrest D 1992 *J. Chem. Phys.* **96** 230
Tarana M and Tennyson J 2008 *J. Phys. B: At. Mol. Opt. Phys.* **41** 205204
Tennyson J 1996 *J. Phys. B: At. Mol. Opt. Phys.* **29** 6185–201
Tennyson J, Brown D B, Munro J J, Rozum I, Varambhia H N and Vinci N 2007 *J. Phys.: Conf. Ser.* **86** 1–12
Tennyson J and Morgan L A 1999 *Phil. Trans. R. Soc.* A **357** 1161–73
Tennyson J and Noble C J 1984 *Comput. Phys. Commun.* **33** 421–4
Turner B E, Chan K W, Green S and Lobowich D A 1992 *Astrophys. J.* **399** 114
Wilson R W, Penzias A A, Jefferts K B, Kutner M and Thaddeus P 1971 *Astrophys. J.* **167** 97